

Distinct photodynamics of κ -N and κ -C pseudoisomeric iron(II) complexes

Philipp Dierks, Ayla Kruse, Olga S. Bokareva, Mohammed J. Al-Marri, Jens Kalmbach, Marc Baltrun, Adam Neuba, Roland Schon, Stephan Hohloch, Katja Heinze, Michael Seitz, Oliver Kühn, Stefan Lochbrunner and Matthias Bauer

Table of Content

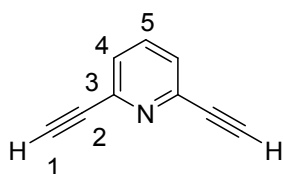
1. Synthesis.....	2
2. Crystallographic data of Fe1 and Fe2	5
3. Quantum-chemical calculations of absorption spectra	9
4. Transient Absorption	9
5. Electrochemical Experiments	10
6. Stationary spectra and details on emission lifetime	11
7. Details on Reactive Oxygen Sensitization	12
8. NMR spectra and MS-data	14
9. References.....	22

1. Synthesis

General aspects of synthesis:

Unless otherwise noted the reactions were performed under argon atmosphere using standard Schlenk techniques. The used solvents were dried and degassed prior to use. All chemicals were purchased from Sigma Aldrich, TCI, Fischer Scientific or abcr. NMR spectra were recorded with a Bruker Avance 700 (^1H , 700.1 MHz; ^{13}C , 176.0 MHz), using different deuterated solvents purchased from Deutero. The NMR signals were referenced to residual solvents measured relative to TMS as internal standard. ESI-MS data were recorded by a Waters Synapt 2G (QTOF). Elemental analyses were performed with a vario MICRO Cube Elementar.

2,6-diethynylpyridine 1:



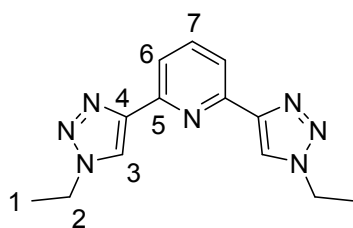
Inspired by literature^[1] 2,6-Dibromopyridine (1184 mg, 5 mmol, 1eq.) and palladium(bis(triphenylphosphan)dichloride) (175 mg, 0.025 mmol, 0.05 eq.) were suspended in NEt_3 (20ml) and degassed by three cycles of freeze, pump, and thaw. Trimethylsilylacetylene (1.6 ml, 11.5 mmol, 2.3 eq.) and copper(I)iodide (48 mg, 0.25 mmol, 0.05 eq.) were added, and the suspension was stirred for 1 d at room temperature and 2 d at 65 °C. The suspension was neutralized by HCl and extracted with DCM. The organic layers were washed with water again. The solvent was removed, and n-hexane was added. The suspension was filtered through a silica plug and TMS-protected product was obtained as white solid. Deprotection was performed with KF (1162 mg, 20 mmol, 10 eq.) in MeOH/THF (30 ml, 1/1 V/V) at room temperature within 16 h. The solution was extracted with DCM and water. The combined organic layers were dried over NaSO_4 and the product was obtained as colorless solid (540 mg, 4.25 mmol, 85 %).

$^1\text{H-NMR}$ (700 MHz, CDCl_3): δ (ppm): 7.63 (t, 1H, $^3J_{\text{HH}} = 7.8$ Hz, H_5); 7.43 (d, 2H, $^3J_{\text{HH}} = 7.8$ Hz, H_4); 3.14 (s, 2H, H_1).

$^{13}\text{C-NMR}$ (176 MHz, CDCl_3): δ (ppm): 142.2 (s, C_q , 2C, C_3); 136.0 (s, 1C, C_5); 126.6 (s, 2C, C_4); 81.5 (s, C_q , 2C, C_2); 77.2 (s, 2C, C_1).

ESI-MS (pos) (m/z in MeCN) calculated for $\text{C}_9\text{H}_5\text{N}$: 127.0422; found: 128.0518 $[\text{M}+\text{H}]^+$.

2,6-bis(1-ethyl-1H-1,2,3-triazol-4-yl)pyridine 2:



Iodoethane (0.26 ml, 3.3 mmol, 3.3 eq.) and sodium azide (585 mg, 9 mmol, 9 eq.) were stirred in a mixture of THF and water for 2 h at room temperature under ambient conditions. 2,6-Diethynylpyridine (127 mg, 1 mmol, 1 eq.), ascorbic acid (141 mg, 0.8 mmol, 0.8 eq.), copper sulfate (64 mg, 0.4 mmol, 0.4 eq.), potassium carbonate (276 mg, 2 mmol, 2 eq.) and pyridine (0.85 ml, 10 mmol, 10 eq.) were added to the *in situ* formed ethyl azide.^[2] The mixture

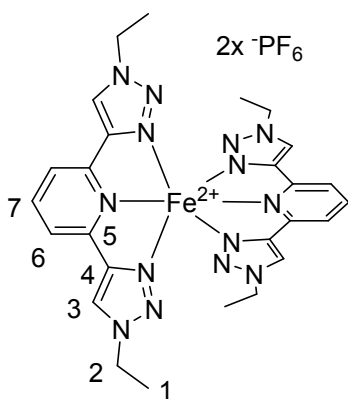
was stirred for 3 d at room temperature under ambient conditions, while arising precipitate was observed. DCM was added to the suspension and was extracted 3x with a saturated NH_3/EDTA solution. The combined organic layers were dried over NaSO_4 , filtered and the solvent was removed under reduced pressure. The crude product was purified by column chromatography (mobile phase: DCM/acetone; 5/1 V/V) and this novel ligand was obtained as a slightly yellow product (186 mg, 0.69 mmol, 69 %).

$^1\text{H-NMR}$ (700 MHz, CDCl_3): δ (ppm): 8.17 (s, 2H, H_3); 8.08 (d, 2H, $^3J_{\text{HH}} = 7.8$ Hz, H_6); 7.84 (t, 1H, $^3J_{\text{HH}} = 7.8$ Hz, H_7); 4.47 (q, 4H, $^3J_{\text{HH}} = 7.3$ Hz, H_2); 1.60 (t, 6H, $^3J_{\text{HH}} = 7.4$ Hz, H_1).

$^{13}\text{C-NMR}$ (176 MHz, CDCl_3): δ (ppm): 150.2 (s, C_q , 2C, C_4); 148.6 (s, C_q , 2C, C_5); 137.8 (s, 1C, C_7); 121.5 (s, 2C, C_3); 119.4 (s, 2C, C_6); 45.6 (s, 2C, C_2); 15.6 (s, 2C, C_1).

ESI-MS (pos) (m/z in MeCN) calculated for $\text{C}_{13}\text{H}_{15}\text{N}_7\text{Na}^+$: 292.1282; found: 292.1309 $[\text{M}+\text{Na}]^+$.

Triazole-Complex Fe1:



2,6-Bis(1-ethyl-1H-1,2,3-triazol-4-yl)pyridine (108 mg, 0.4 mmol, 2 eq.) and FeBr_2 (43 mg, 0.2 mmol, 1 eq.) were stirred in degassed EtOH (20 ml) for 16 h. Insoluble solid was filtered, the filtrate was concentrated and dropped into an aqueous KPF_6 solution (0.1 M, 368 mg, 2 mmol in 20 ml water). Arising precipitate was filtered and washed with water. The crude product was solved in acetone and precipitated in diethylether. After filtering, the product was purified by crystallization via solvent diffusion (DMSO/water) and the final novel complex was obtained as red needles (131 mg, 0.148 mmol, 74%).

$^1\text{H-NMR}$ (700 MHz, d_6 -acetone): δ (ppm): 9.28 (s, 4H, H_3); 8.94 (d, $^3J_{\text{HH}} = 6.0$ Hz, H_6); 8.53 (t, $^3J_{\text{HH}} = 7.9$ Hz, H_7); 4.46 (q, $^3J_{\text{HH}} = 7.3$ Hz, H_2); 1.36 (t, $^3J_{\text{HH}} = 7.9$ Hz, H_1).

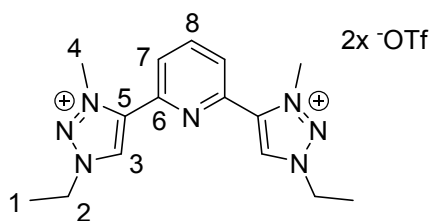
$^{13}\text{C-NMR}$ (176 MHz, CDCl_3): δ (ppm): 153.3 (s, C_q , 4C, C_4); 149.0 (s, C_q , 4C, C_5); 140.7 (s, 2C, C_7); 125.6 (s, 4C, C_3); 123.4 (s, 4C, C_6); 49.0 (s, 4C, C_2); 15.2 (s, 4C, C_1).

ESI-MS (pos) (m/z in MeCN) calculated for $\text{C}_{26}\text{H}_{30}\text{FeN}_{14}^{2+}$: 297.1058; found: 297.1108 $[\text{M}]^{2+}$.

Elemental analysis calculated for $\text{C}_{26}\text{H}_{30}\text{F}_{12}\text{FeN}_{14}\text{P}_2$: C = 35.31 %, H = 3.42 %, N = 22.17 %.

Found: C = 35.34 %, H = 3.74 %, N = 22.14 %.

4,4'-(pyridine-2,6-diyl)bis(1-ethyl-3-methyl-1H-1,2,3-triazol-3-ium)triflate **3**:



Inspired by literature^[3] 2,6-Bis(1-ethyl-1H-1,2,3-triazol-4-yl)pyridine (269 mg, 1 mmol, 1 eq.) was dissolved in DCM (10 ml) and cooled to -80 °C. MeOTf (0.25 ml, 2.2 mmol, 2.2 eq.) was added dropwise. The reaction mixture was stirred for 16 h while slowly warming to room temperature. The arising precipitate was filtered and washed with *n*-pentane. The product was purified by crystallization via solvent diffusion

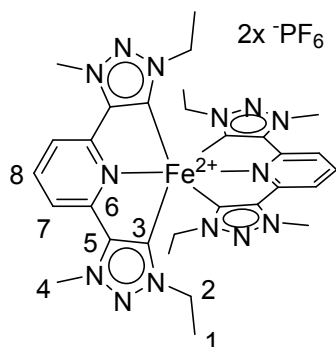
(acetone/ diethylether) and this novel pre-ligand was obtained as colourless crystals (549 mg, 0.92 mmol, 92 %).

¹H-NMR (700 MHz, *d*₆-acetone): δ (ppm): 9.52 (s, 2H, H₃); 8.42 (t, 1H, ³J_{HH} = 7.9 Hz, H₈); 8.35 (d, 2H, ³J_{HH} = 8.2 Hz, H₇); 4.88 (q, 4H, ³J_{HH} = 7.4 Hz, H₂); 4.75 (s, 6H, H₄); 1.74 (t, 6H, ³J_{HH} = 7.4 Hz, H₁).

¹³C-NMR (176 MHz, *d*₆-acetone): δ (ppm): 144.9 (s, C_q, 2C, C₆); 141.4 (s, 1C, C₈); 131.1 (s, C_q, 2C, C₅); 131.0 (s, 2C, C₃); 127.6 (s, 2C, C₇); 122.2 (quartet, 2C, C_{triflate}); 50.6 (s, 2C, C₂); 41.5 (s, 2C, C₄); 14.6 (s, 2C, C₁).

ESI-MS (pos) (m/z in MeCN) calculated for C₁₅H₂₁N₇²⁺: 149.5924; found: 149.5960 [M]²⁺.

Triazolylidene-Complex **Fe2**:



4,4'-(Pyridine-2,6-diyl)bis(1-ethyl-3-methyl-1H-1,2,3-triazol-3-ium)triflate (120 mg, 0.2 mmol, 2 eq.) was suspended in THF (10 ml) and cooled to -80 °C. LiHMDS (0.6 ml, 1 M in THF, 0.6 mmol, 6 eq.) was added dropwise. Complete deprotonation of the ligand precursor was observed after about 1 h resulting in a clear solution. FeBr₂ (22 mg, 0.1 mmol, 1 eq.) was suspended in THF (5 ml) and added dropwise to the solution prepared before. The solution immediately turned dark and was then stirred for 16 h while slowly warming to room temperature. This procedure is according to previously described synthesis.^[3] Insoluble solid was filtered and washed with acetone, the filtrate was concentrated and dropped into an aqueous KPF₆ solution

(0.1 M, 184 mg, 1 mmol in 10 ml water). Arising precipitate was filtered and washed with water. The crude product was dissolved in acetone and precipitated in diethylether. After filtering, the product was purified by crystallization via solvent diffusion (acetone/ diethylether) and the novel complex was obtained as blue needles (44 mg, 0.046mmol, 46 %).

¹H-NMR (700 MHz, *d*₆-DMSO): δ (ppm): 8.04 (m, 6H, H₇ & H₈); 4.52 (s, 12H, H₄); 3.15 (q, 8H, ³J_{HH} = 7.3 Hz, H₂); 0.67 (t, 12H, ³J_{HH} = 7.3 Hz, H₁).

¹³C-NMR (176 MHz, *d*₆-DMSO): δ (ppm): 191.1 (s, C_q, 4C, C₃); 152.5 (s, 4C, C₆); 143.1 (s, 4C, C₅); 133.0 (s, 2C, C₈); 116.3 (s, 4C, C₇); 46.7 (s, 4C, C₂); 15.4 (s, 4C, C₁).

ESI-MS (pos) (m/z in MeCN) calculated for C₃₀H₃₈FeN₁₄²⁺: 325.1371; found: 325.1389 [M]²⁺.

Elemental analysis calculated for (C₃₀H₃₈F₁₂FeN₁₄P₂)₃(C₄H₁₀O): C = 38.99 %, H = 4.32 %, N = 20.32 %.

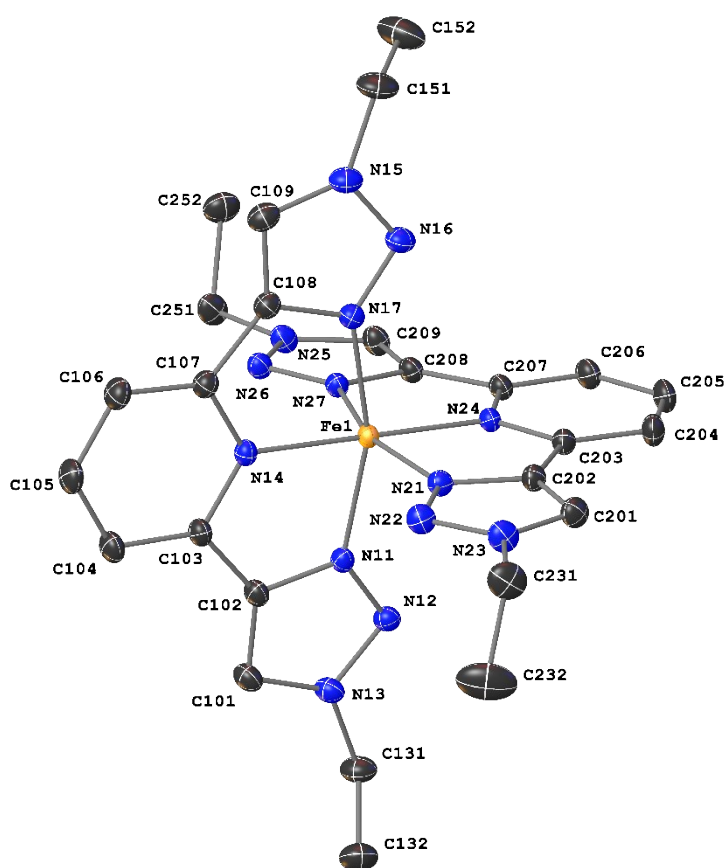
Found: C = 38.60 %, H = 4.70 %, N = 20.60 %.

2. Crystallographic data of Fe1 and Fe2

The X-ray single crystal data were recorded on a Bruker Venture D8 diffractometer, equipped with a Mo K α μ S 3.0-source ($\lambda=0.71073$ Å) and a Photon III area detector at 120 K. The obtained data were integrated with SAINT and a multi-scan absorption correction was carried out by SADABS. The structure solution by direct methods and the refinement of the structures using full-matrix least squares method based on F^2 were achieved in SHELX – all three software programs are parts of the Bruker APEX III package.^[4] All non-hydrogen-atoms were refined anisotropically and the hydrogen atom positions at idealized positions residing on the carbon atoms with isotropic displacement parameters $U_{iso}(H)=1.2$ Ueq(C) resp. 1.5 Ueq(-CH₃) and C-H bond lengths of 0.93-0.96 Å. All CH₃ hydrogen atoms were allowed to rotate but not to tip.

Crystallographic data have been deposited at the Cambridge Crystallographic Data Centre assigned to the deposition number CCDC 2050317 (**Fe1**) and 2049729 (**Fe2**). Copies are available free of charge via www.ccdc.cam.ac.uk.

Fe1:



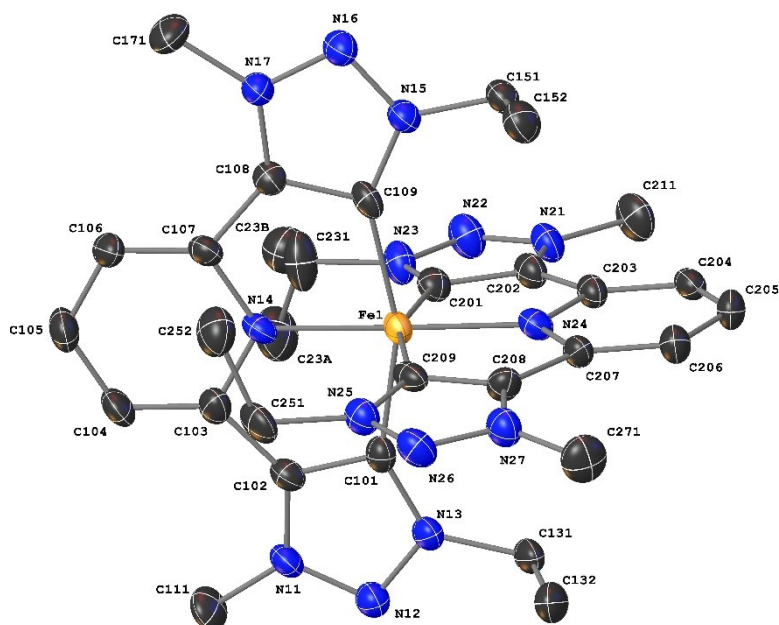
CCDC number

2050317

Empirical formula

C₂₆ H₃₀ F₁₂ Fe N₁₄ P₂

Formula weight	884.43	
Temperature	120(2) K	
Wavelength	0.71073 Å	
Crystal system	Triclinic	
Space group	P-1	
Unit cell dimensions	a = 11.6525(6) Å	$\alpha = 92.055(2)^\circ$.
	b = 13.4838(7) Å	$\beta = 103.119(2)^\circ$.
	c = 13.7533(7) Å	$\gamma = 111.670(2)^\circ$.
Volume	1938.61(18) Å ³	
Z	2	
Density (calculated)	1.515 Mg/m ³	
Absorption coefficient	0.569 mm ⁻¹	
F(000)	896	
Crystal size	0.30 x 0.12 x 0.10 mm ³	
Theta range for data collection	1.947 to 31.575°.	
Index ranges	-17<=h<=17, -19<=k<=19, -20<=l<=20	
Reflections collected	273411	
Independent reflections	12923 [R(int) = 0.0359]	
Completeness to theta = 25.242°	99.5 %	
Absorption correction	Semi-empirical from equivalents	
Refinement method	Full-matrix least-squares on F ²	
Data / restraints / parameters	12923 / 0 / 500	
Goodness-of-fit on F ²	1.038	
Final R indices [I>2sigma(I)]	R1 = 0.0310, wR2 = 0.0797	
R indices (all data)	R1 = 0.0352, wR2 = 0.0837	
Extinction coefficient	n/a	
Largest diff. peak and hole	0.720 and -0.612 e.Å ⁻³	

Fe2:

CCDC number	2049729	
Empirical formula	C ₃₁ H ₄₀ F ₁₂ Fe N ₁₄ P ₂ Cl ₂	
Formula weight	1025.44	
Temperature	130(2) K	
Wavelength	0.71073 Å	
Crystal system	Monoclinic	
Space group	P 1 21/c 1	
Unit cell dimensions	a = 8.5217(14) Å	α = 90°.
	b = 36.898(6) Å	β = 94.519(3)°.
	c = 13.416(2) Å	γ = 90°.
Volume	4205.4(12) Å ³	
Z	4	
Density (calculated)	1.620 Mg/m ³	
Absorption coefficient	0.660 mm ⁻¹	
F(000)	2112	
Crystal size	0.25 x 0.24 x 0.21 mm ³	

Theta range for data collection	1.620 to 25.528°.
Index ranges	-10<=h<=10, -44<=k<=44, -16<=l<=16
Reflections collected	46215
Independent reflections	7782 [R(int) = 0.1377]
Completeness to theta = 25.242°	99.7 %
Absorption correction	Semi-empirical from equivalents
Max. and min. transmission	0.7452 and 0.6344
Refinement method	Full-matrix least-squares on F ²
Data / restraints / parameters	7782 / 0 / 548
Goodness-of-fit on F ²	0.954
Final R indices [I>2sigma(I)]	R1 = 0.0591, wR2 = 0.1354
R indices (all data)	R1 = 0.0981, wR2 = 0.1457
Extinction coefficient	n/a
Largest diff. peak and hole	0.814 and -0.545 e.Å ⁻³

Table S 1: Selected structural parameters of **Fe1**, [Fe(tpy)₂]²⁺, [Fe(bpy)₃]²⁺, **Fe2**, [Fe(bim)₂]²⁺ and [Fe(bpy)(btz)₂]²⁺.

	N-Fe-N [°]	C-Fe-C [°]	Fe-N _{pyridine} [Å]	Fe-C _{carbene} [Å]	Ref.
Fe1	161.06(4)	-	1.9539(9)	-	This work
[Fe(tpy) ₂] ²⁺	161.55(12)	-	1.987(3)	-	Ref. ^[5]
[Fe(bpy) ₃] ²⁺	174.61	-	1.9670(4)	-	Ref. ^[6]
Fe2	-	159.68(17)	1.956(3)	1.956(3)	This work
[Fe(bim) ₂] ²⁺	-	158.32(15)	1.925(3)	1.9665(3)	Ref. ^[7]
[Fe(bpy)(btz) ₂] ²⁺	-	173.0(7)	-	1.967(17)	Ref. ^[8]

3. Quantum-chemical calculations of absorption spectra

Absorption spectra were computed with linear-response time-dependent density functional theory (TDDFT) using the optimally-tuned LC-BLYP functional together with the polarizable continuum model (PCM) to account for solvent effects (acetonitrile). The two-parameter optimal tuning of LC-BLYP was done via the Δ SCF method,^[9] the details of the present setup can be found in the literature.^[10] The 6-31G(d) basis set was used for the tuning procedure, while a larger basis set (def2-TZVP on Fe, 6-311G(d,p) on other atoms) was employed for calculations of absorption spectra. For each molecule, 100 singlet and 100 triplet excited states were computed. The broadening of the resulting stick spectra was done by Gaussians with a width (FWHM) of 0.15 eV. All calculations were performed with the Gaussian16 suite of programs.^[11] Excited state analysis was performed using the TheoDORE package,^[12] which enables automatic quantitative wavefunction analysis and localization of excitations at predefined molecular moieties. Pre- and post-processing of the data was done with homemade programs.

4. Transient Absorption

Transient absorption spectra were recorded with a time resolution of about 100 fs by means of a pump-probe setup. In the setup, a non-collinear optical parametric amplifier (NOPA) tuned to a centre wavelength of 490 nm for complex **Fe1** and 600 nm for complex **Fe2** was applied to excite the sample. A white light continuum was generated in a CaF₂ crystal for probing.^[13] Both, the NOPA and the white light stage were pumped by a regenerative Ti:sapphire laser system (CPA 2001, Clark MXR, Inc.) operating at a centre wavelength of 775 nm with a repetition rate of 1 kHz. The dispersion of the NOPA pulses was minimized by a compressor based on fused silica prisms. To avoid effects caused by orientational relaxation, the polarizations of the pump and probe pulses were set to magic angle with respect to each other. Pump and probe beam were focused onto the sample to overlapping spots with diameters of approximately 400 μ m and 100 μ m, respectively. Behind the sample, the probe was dispersed by a prism and transient absorption changes were spectrally resolved recorded by a photodiode array detector. The compounds were dissolved in MeCN under argon and the sample solution was filled into a fused silica cuvette with a thickness of 1 mm.

5. Electrochemical Experiments

Potentiometric measurements were performed in deoxygenated MeCN at room temperature using a PGSTAT 101 potentiostat from Metrohm-Autolab. An analyte concentration of 10^{-3} M and a $[n\text{-Bu}_4\text{N}][\text{PF}_6]$ concentration of 0.1 M as inert electrolyte were used. In a three-electrode configuration, a Pt working electrode (1 mm diameter), Ag/0.01 M AgNO₃, 0.1 M $[n\text{-Bu}_4\text{N}][\text{PF}_6]$ in MeCN as reference electrode, and a Pt pin as a counter electrode were applied. After the measurements, ferrocene FcH was added as an internal standard to reference against the FcH/FcH⁺ redox couple. The resulting voltammograms were analyzed using the software Nova 2.1.3. The reversibility of the redox couples was checked by using the criteria from Nicholson^[14] and the Randles-Sevcik-equation.^[15]

Spectroelectrochemical and coulometric measurements were performed at room temperature in an optically transparent cell ($d = 1$ mm) using a deoxygenated MeCN/0.1 M $[n\text{-Bu}_4\text{N}][\text{PF}_6]$ solution and a Pt wire mesh working electrode (counter electrode: Pt wire). Spectral changes during oxidations/reductions were recorded on a Varian Cary 50 spectrophotometer.

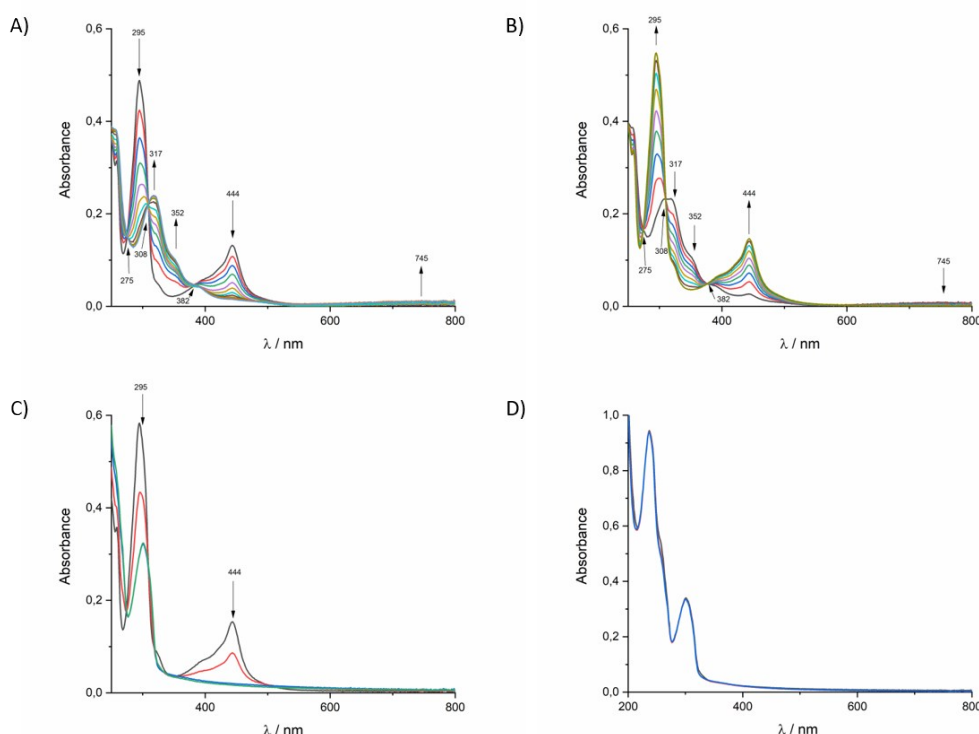


Figure S 1: Changes in the UV/vis spectra of **Fe1** during A) oxidation with an applied potential of 1.34 V B) re-reduction with an applied potential of 0.6 V C) ligand reduction with an applied potential of -2.34 V and D) ligand re-oxidation with an applied potential of 0 V.

As seen in Figure S 1, the Fe^{II/III} oxidation in **Fe1** is reversible as the ground state absorption spectrum is recovering in the re-reduction process. The reduction of the ligand shown in panel C) leads to a bleaching of the MLCT absorption, which is not recovering after applying a re-oxidation potential as shown in D). Accordingly, reduction of the ligand seems to be irreversible and the spectrum of the reduced species is not taken into consideration to model the decay associated spectra (DAS) of **Fe1**.

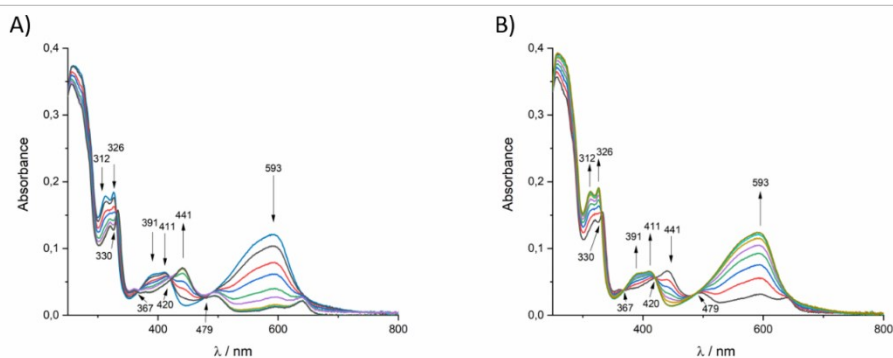


Figure S 2: Changes in the UV/vis spectra of **Fe2** during A) oxidation with an applied potential of 0.2 V B) re-reduction with an applied potential of -0.3 V.

Figure S 2 shows the spectral changes after $\text{Fe}^{\text{II/III}}$ oxidation in **Fe2** in panel A). In panel B), the ground state recovery after the re-reduction process is depicted. Due to this observation, the $\text{Fe}^{\text{II/III}}$ redox couple is expected to be fully reversible.

6. Stationary spectra and details on emission lifetime

Absorption spectra were recorded at concentrations of 10^{-5} M on a PerkinElmer Lambda 465 single beam spectrophotometer. The emission spectra were recorded using a Jasco FP-8300 fluorometer. Spectroscopy grade solvents from VWR and quartz cuvettes by Hellma with a pathlength of 1 cm were used. Luminescence lifetimes were measured on a Horiba Ultima-01-DD (HORIBA Jobin Yvon GmbH) applying the time-correlated single photon counting (TCSPC) technique. **Fe1** was excited at 274 nm (Horiba DeltaDiode-300 LED, 20 MHz, HORIBA Jobin Yvon GmbH) and the emission was recorded at the given luminescence maximum $\lambda_{\text{em}} = 334$ nm until the peak signal reached 10,000 counts. Decay data analysis was performed using the DAS6 software (version v 6.8, HORIBA Scientific). The goodness of the fits was evaluated by χ^2 values (see insets B and C in Figure S 3). As result, an emission band with a maximum at $\lambda_{\text{em}} = 334$ nm is observed after excitation at 295 nm. The emission lifetimes after excitation at 274 nm are determined to be $\tau_{\text{em,ambient}} = 2.6$ ns (Inset B) under ambient conditions and $\tau_{\text{Em,de aerated}} = 2.9$ ns (Inset C) for degassed sample.

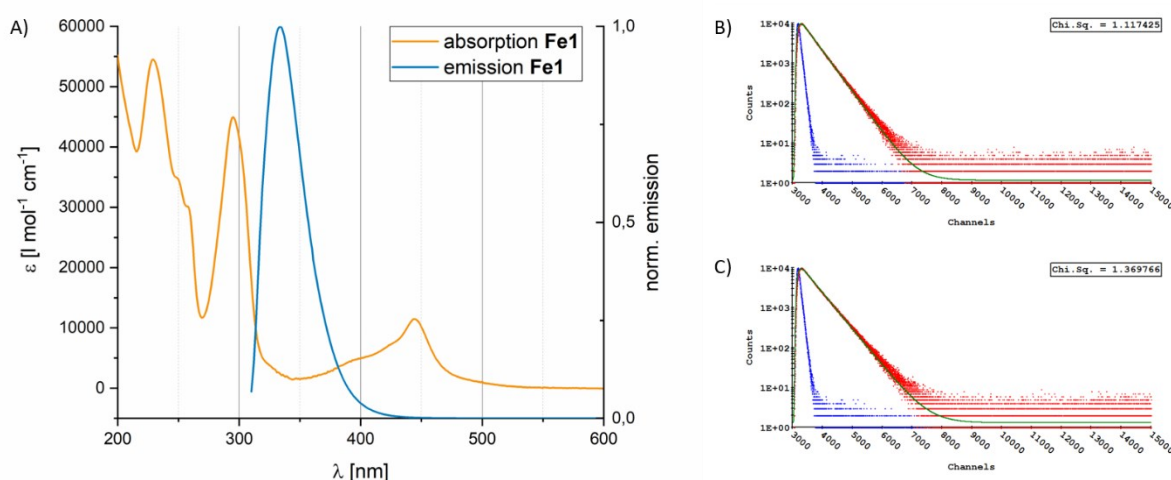
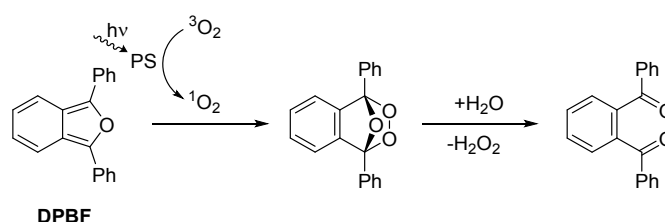


Figure S 3: A) Ground state absorption of **Fe1** and excited state emission after excitation with $\lambda_{\text{ex}} = 295$ nm. Emission lifetimes are determined by TCSPC after excitation with $\lambda_{\text{ex}} = 274$ nm to be B) $\tau_{\text{em,gassed}} = 2.6$ ns under ambient conditions and C) $\tau_{\text{em,de aerated}} = 2.9$ ns under deaerated conditions. χ^2 values are given in the insets.

7. Details on Reactive Oxygen Sensitization

The reaction of 1,3-diphenyl-isobenzofuran (**DPBF**) with $^1\text{O}_2$ was used to indirectly detect the presence of non-luminescent high spin states. The measurements were carried out at room temperature in air saturated MeOH. 2.5 mL **DPBF** (20 μM) were mixed with 0.5 mL complex (10⁻⁴ M) in a 1 cm path Hellma fluorescence cuvette and illuminated with $\lambda = 480 \pm 5$ nm in a Jasco FP-8300 fluorescence spectrophotometer. The consumption of **DPBF** was detected by monitoring the decreasing luminescence intensity at 475 nm after excitation with $\lambda_{\text{ex}} = 405 \pm 5$ nm. The emission was recorded in a range from 425-600 nm with a scan speed of 500 nm/min. $[\text{Ru}(\text{bpy})_3]^{2+}$ as an effective $^1\text{O}_2$ sensitizer in air-saturated MeOH was used as a reference.^[16]



Scheme S 1: Reaction of DPBF with reactive oxygen in presence of a photosensitizer with long-lived triplet excited state.

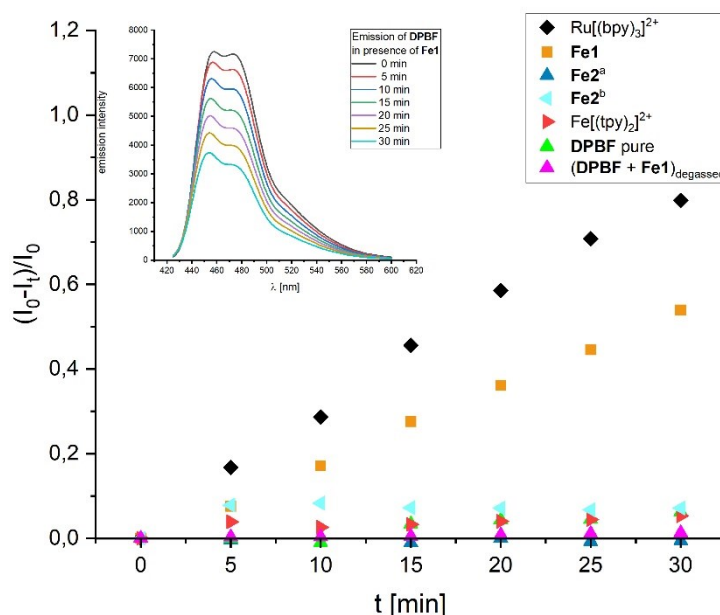


Figure S 4: **DPBF** consumption as function of irradiation time ($\lambda_{\text{ir}} = 480$ nm) in air equilibrated MeOH. Inset: time dependent emission spectra of the system with **Fe1**. **Fe2** has been probed with ^{a)} $\lambda_{\text{ex}} = 480$ nm and ^{b)} $\lambda_{\text{ex}} = 590$ nm.

As shown in Figure S 4, the decomposition reaction of DPBF is effectively initialized by $[\text{Ru}(\text{bpy})_2]^{2+}$ and **Fe1**. Therefore, we assume singlet oxygen sensitization for these two complexes. **DPBF** without any additional photosensitizer and **DPBF + Fe1** in a degassed solution show no decomposition of **DPBF**. **Fe2** does not show oxygen sensitization after excitation with a) $\lambda_{\text{ex}} = 480$ nm and b) $\lambda_{\text{ex}} = 590$ nm. Additionally, the ability of $[\text{Fe}(\text{tpy})_2]^{2+}$ to sensitize oxygen was tested, but no decomposition of DPBF was detected. This leads to the interpretation, that **Fe1** could be ending up in a long-lived triplet state after photoexcitation in the MLCT band and is probably not resulting in a long-lived ^5MC state like $[\text{Fe}(\text{tpy})_2]^{2+}$. This interpretation strongly needs to be clarified by further investigations.

Singlet oxygen near-IR luminescence measurements were performed on a Horiba Fluorolog-3 spectrofluorimeter equipped with a 450 W Xenon lamp for steady-state measurements. Emitted light was detected by a Hamamatsu H10330-75 PMT detector ($950 \text{ nm} < \lambda_{\text{em}} < 1700 \text{ nm}$). Spectral selection in the excitation path was accomplished by a DFX monochromator (double gratings: 1200 grooves/mm, 330 nm blaze) and in the emission path in the NIR spectral region ($\lambda_{\text{em}} > 950 \text{ nm}$) by a spectrograph iHR320 (single grating: 600 grooves/mm, 1000 nm blaze). The luminescence band at 1270 nm was, characteristic of singlet oxygen, measured in quartz cuvettes (Suprasil, pathlength 1.0 cm) on air-saturated solutions of **Fe1** in CD_3OD (99.8 %D) at room temperature.

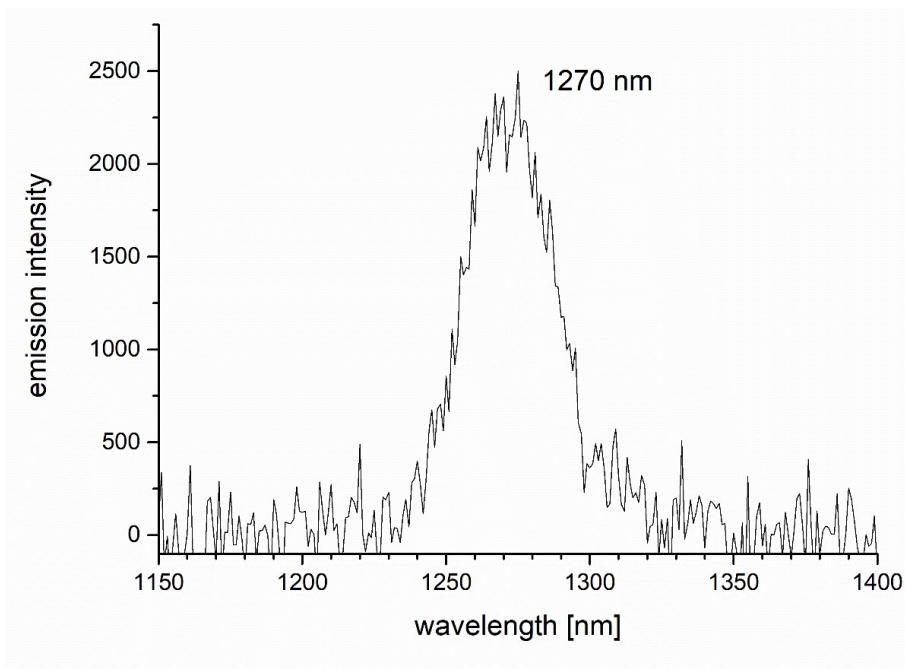


Figure S 5: Steady-state emission spectrum of an air-saturated CD_3OD solution of **Fe1** ($c \approx 10^{-5} \text{ M}$) at room temperature ($\lambda_{\text{ex}} = 275 \text{ nm}$).

The combination of the two strategies to show singlet oxygen sensitization and quantum chemical calculations on **Fe1** reveals that both probed transitions (MLCT-transition at 480 nm and π - π^* -transition at 295 nm) might result in the same ligand centered excited state (molecular orbital plots shown at the top of Fig. S6). For this reason, we assume that both excited states might evolve to the

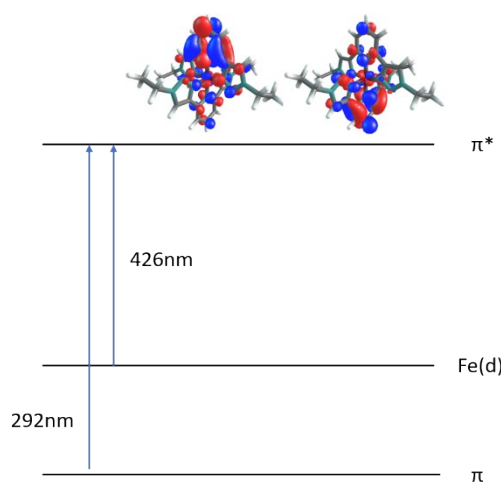
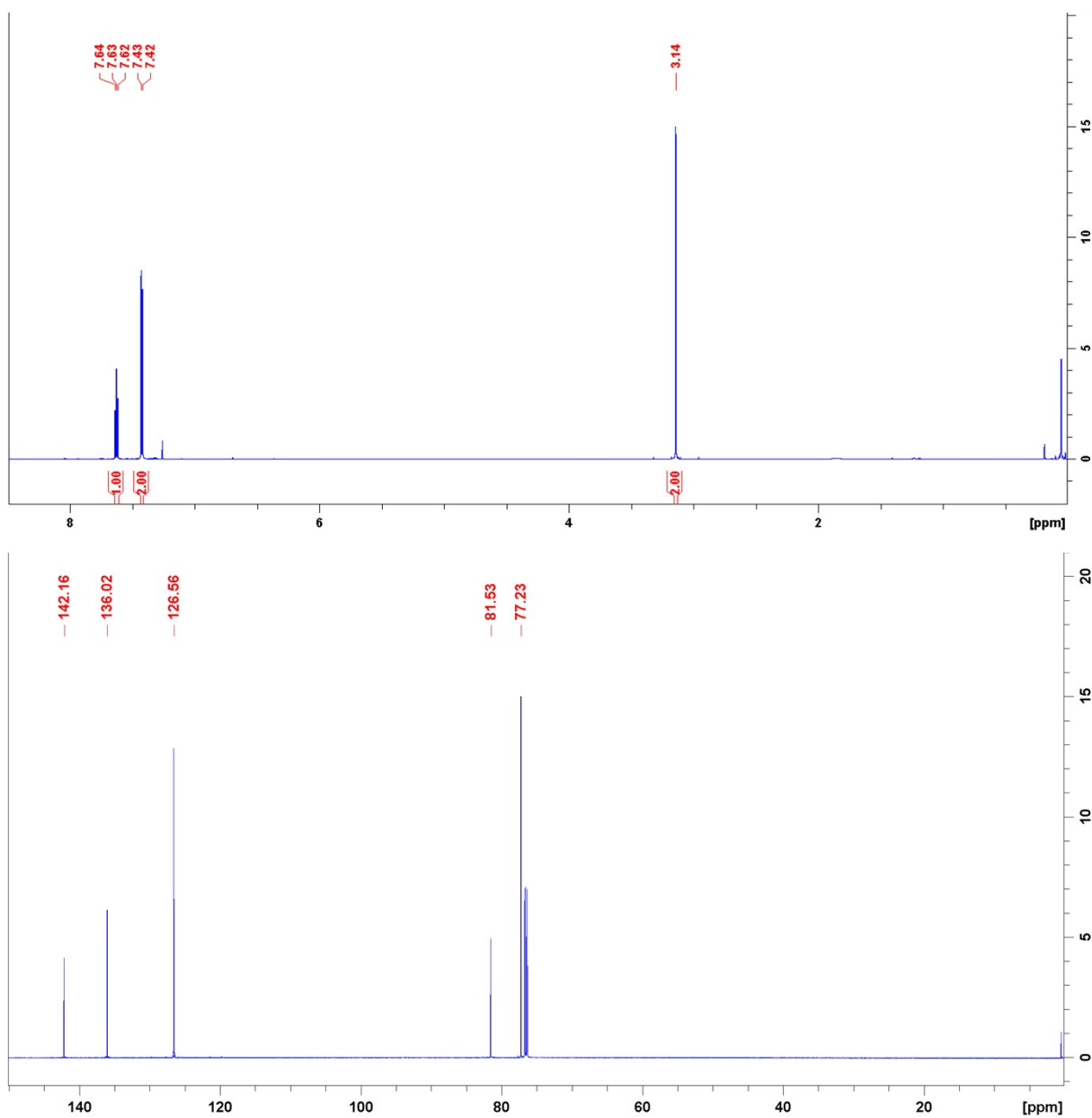


Figure S 6: Plot of the target molecular orbitals populated after calculated transitions with 426 nm and 292 nm.

same dark excited state, which is able to sensitize oxygen, within the relaxation cascade.

8. NMR spectra and MS-data

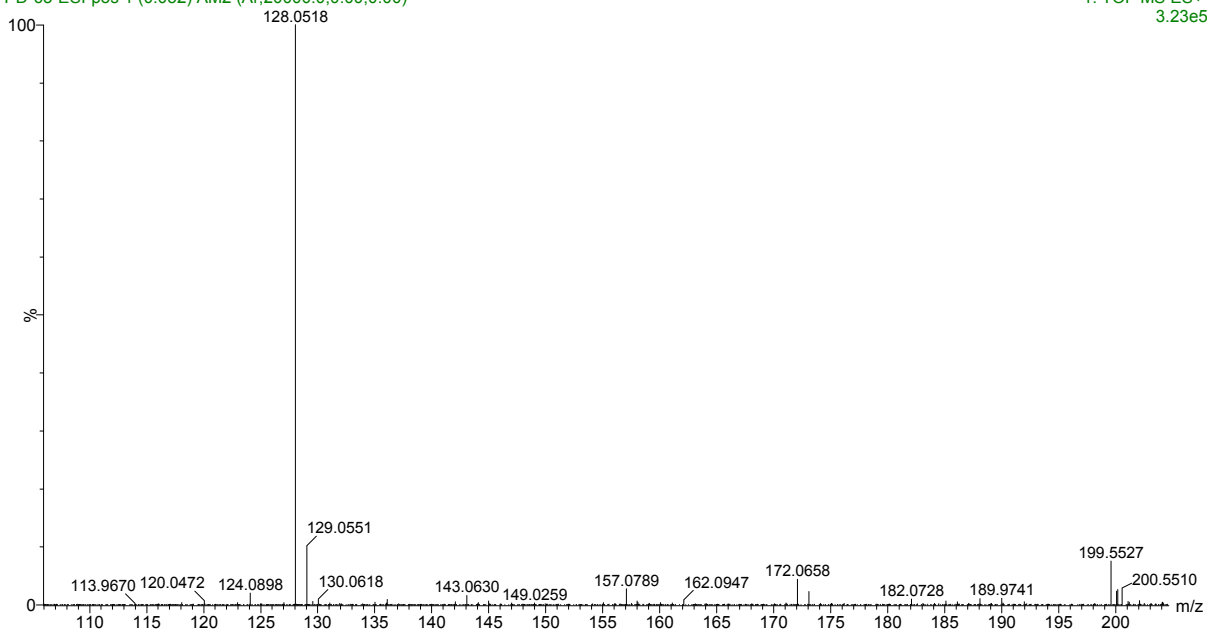
2,6-diethynylpyridine 1 CDCl₃:



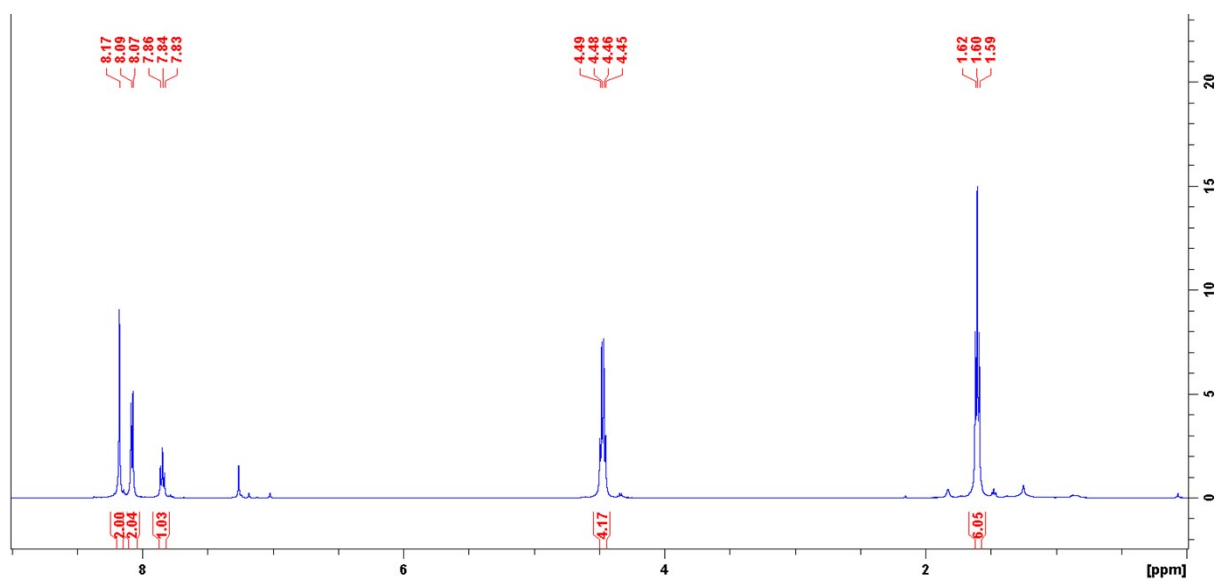
MeCN-CHCl3

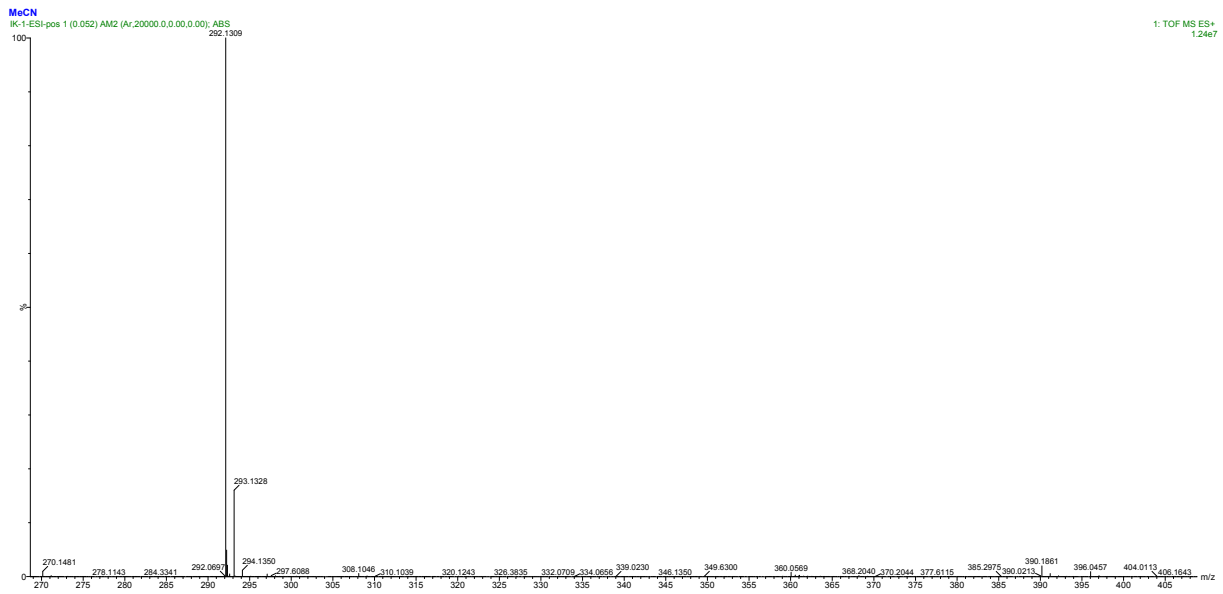
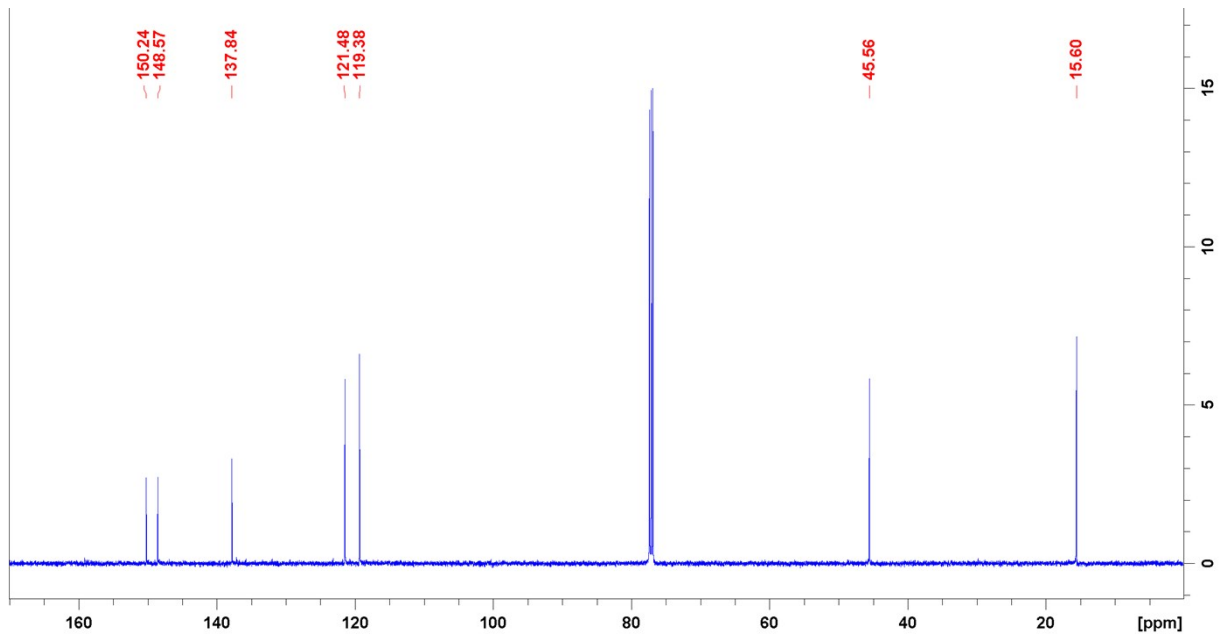
PD-63-ESI-pos 1 (0.052) AM2 (Ar,20000,0,0.00,0.00)

1: TOF MS ES+
3.23e5

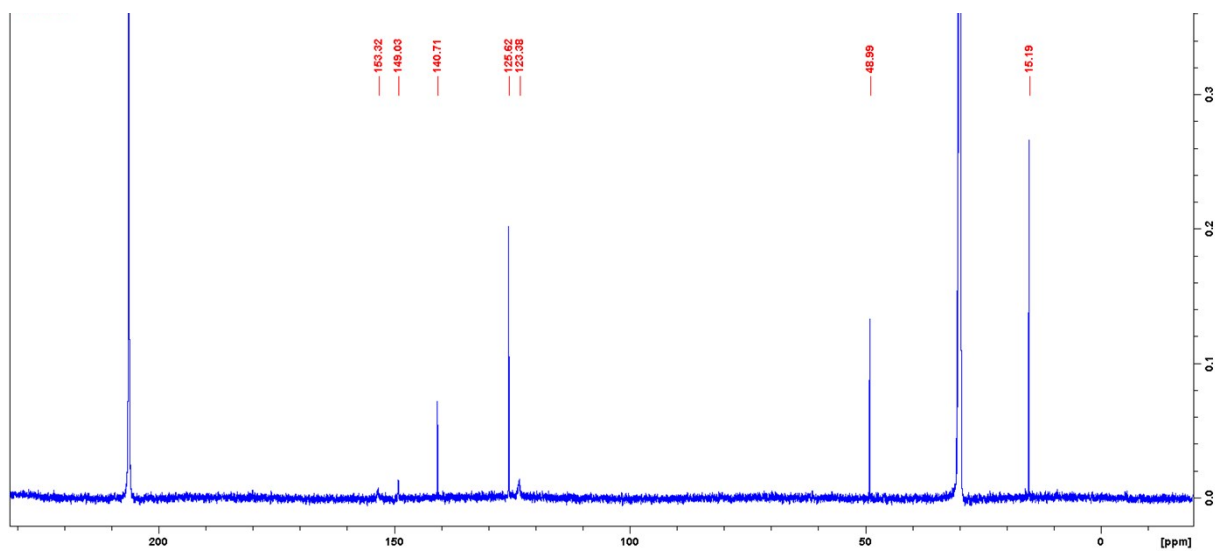
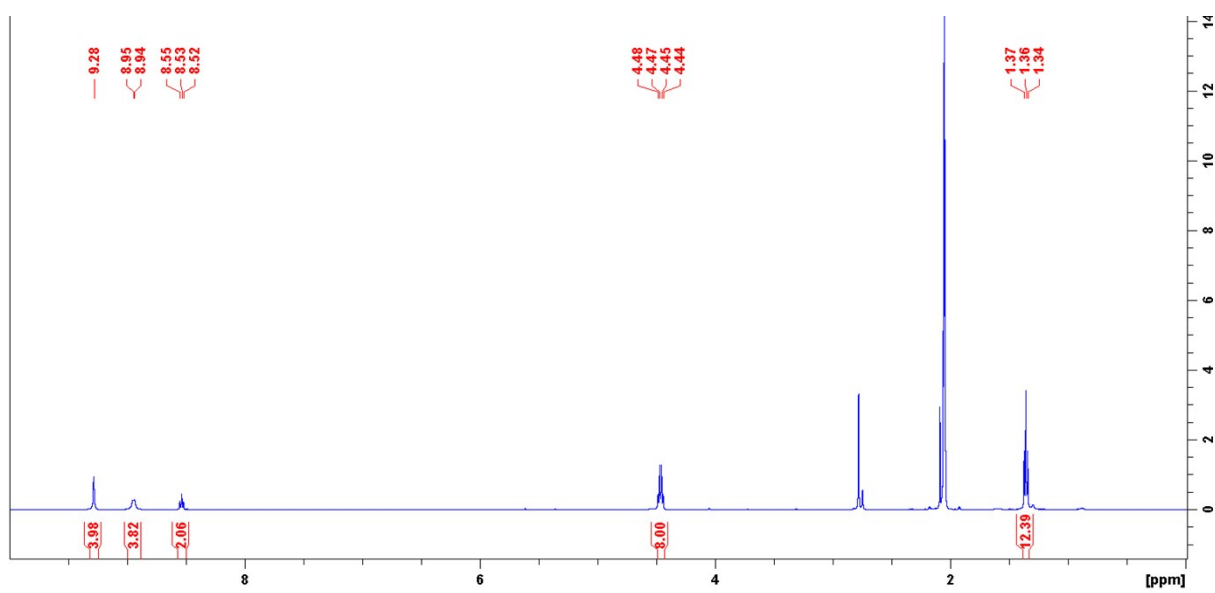


2,6-bis(1-ethyl-1H-1,2,3-triazol-4-yl)pyridine **2** in CDCl₃:





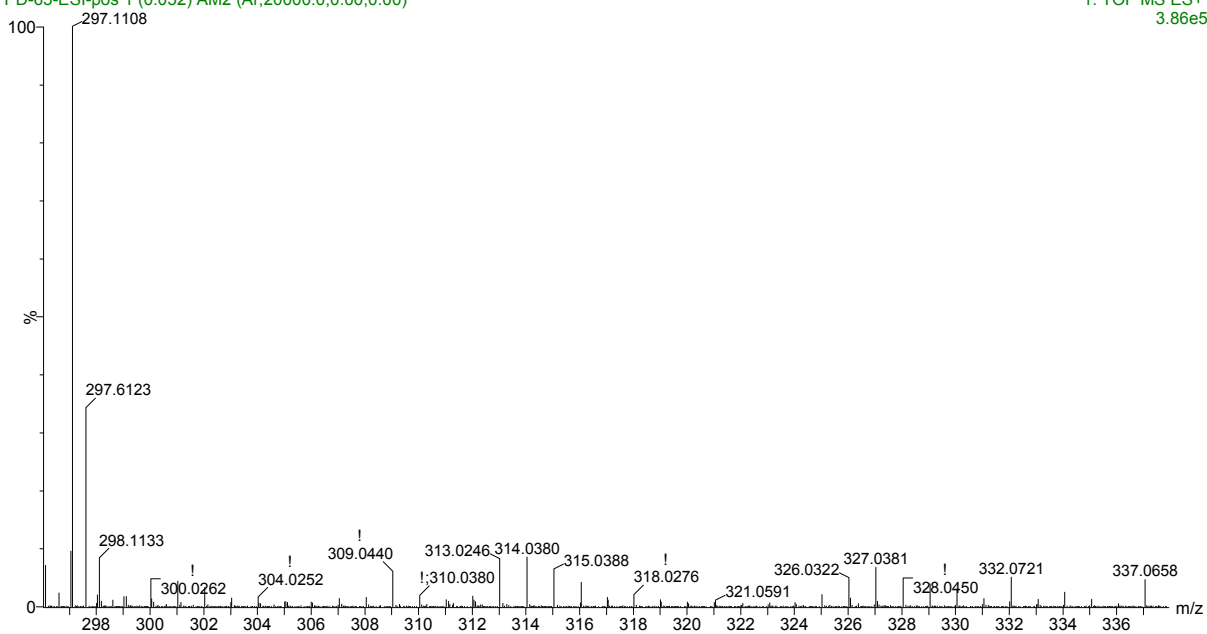
Triazole-Complex **Fe1** in d₆-acetone:



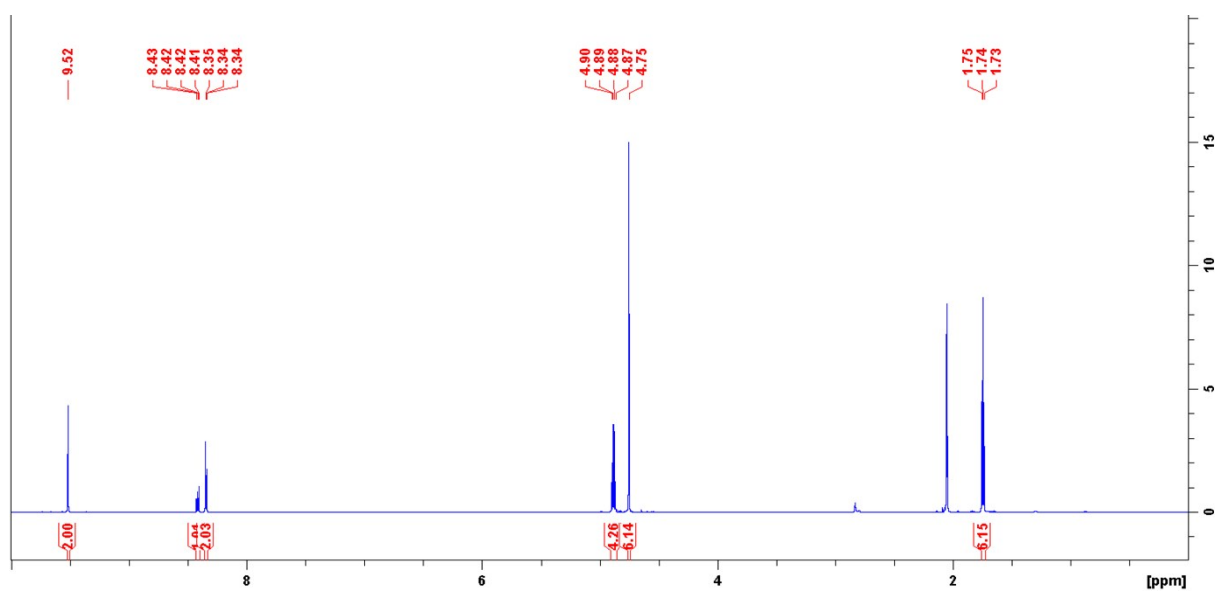
MeCN

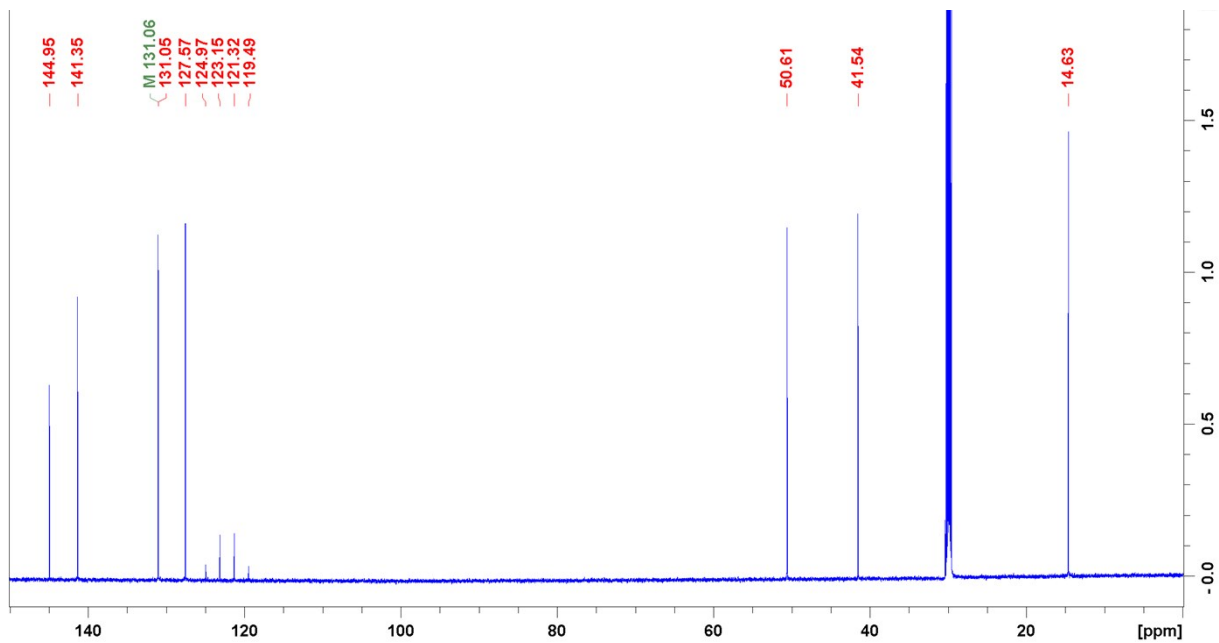
PD-65-ESI-pos 1 (0.052) AM2 (Ar,20000.0,0.00,0.00)

1: TOF MS ES+
3.86e5



4,4'-(pyridine-2,6-diyl)bis(1-ethyl-3-methyl-1H-1,2,3-triazol-3-ium)triflate **3** in d_6 -acetone:

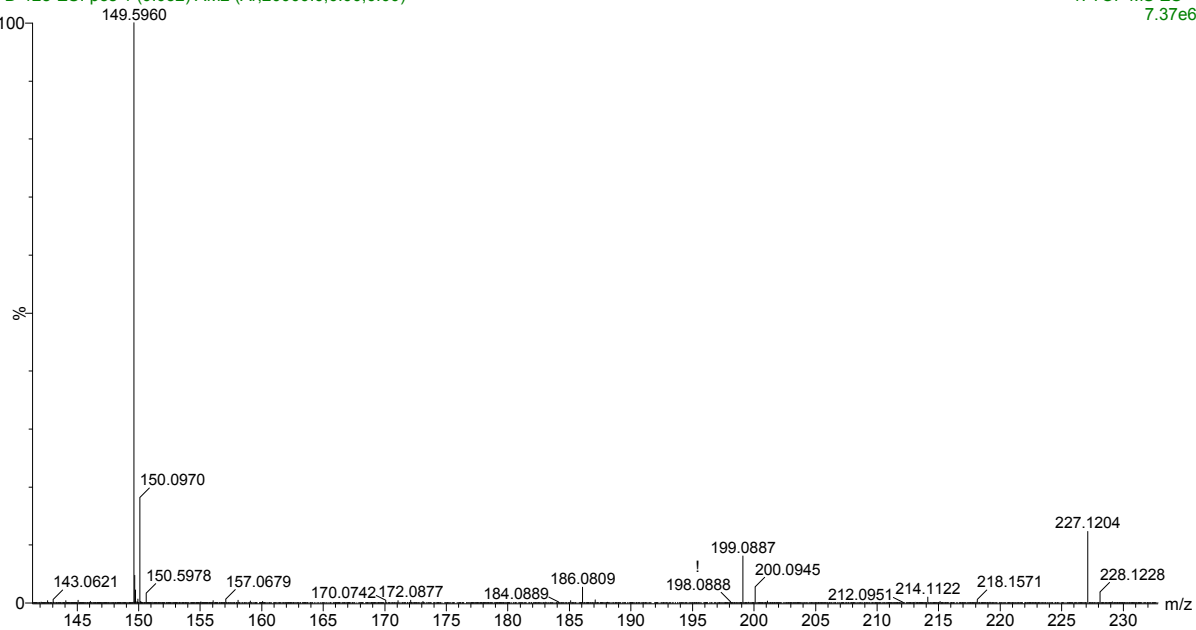




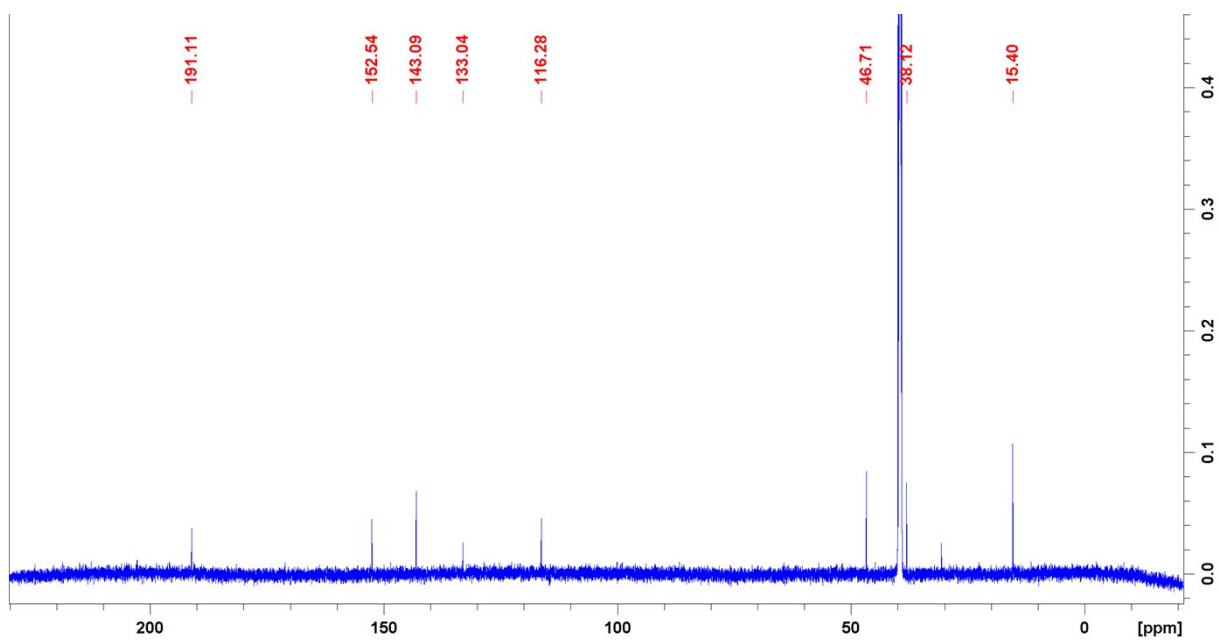
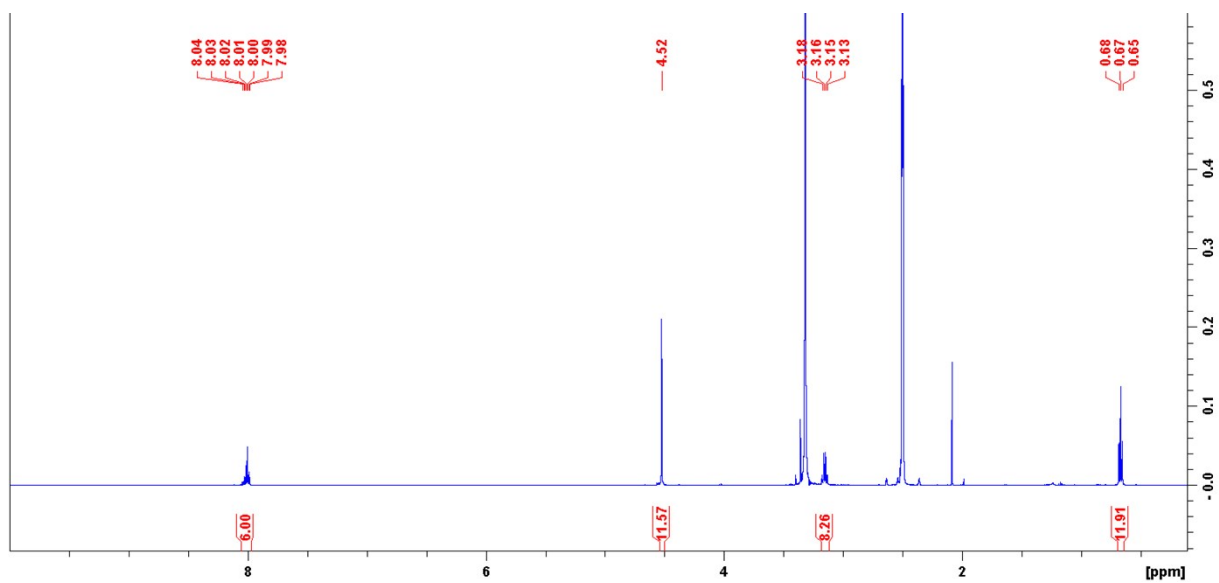
MeCN

PD-128-ESI-pos 1 (0.052) AM2 (Ar,20000.0,0.00,0.00)

1: TOF MS ES+
7.37e6



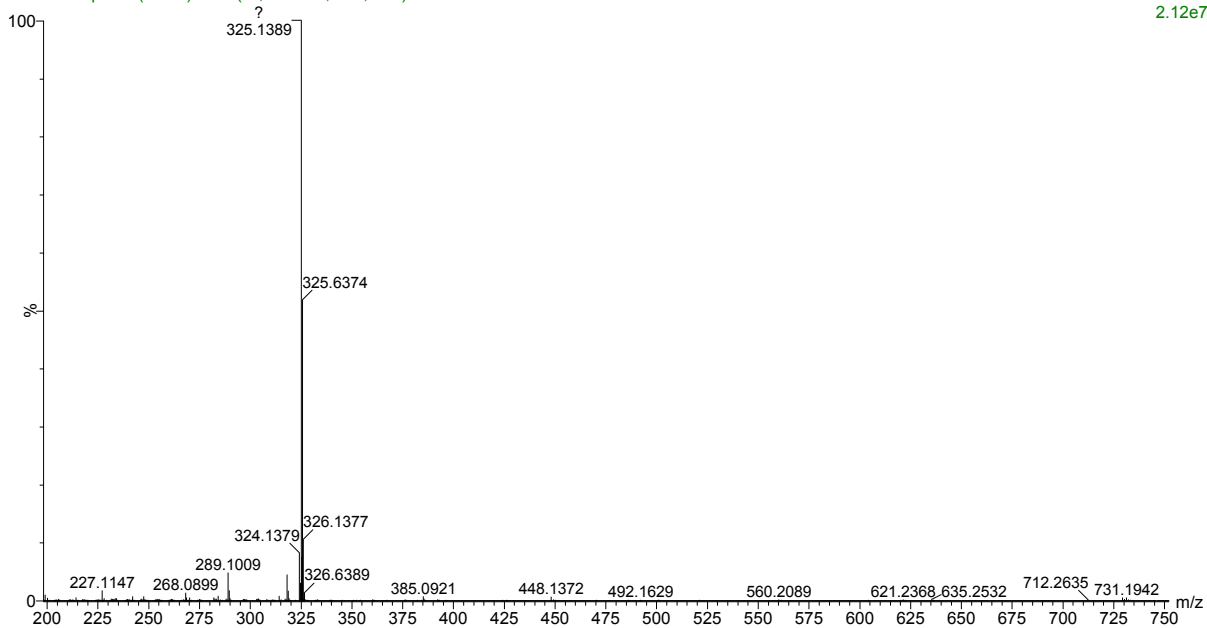
Triazolylidene-Complex **Fe2** in d₆-DMSO:



MeCN

PD-60-ESI-pos 1 (0.052) AM2 (Ar,20000.0,0.00,0.00)

1: TOF MS ES+
2.12e7



9. References

- [1] A. Orita, T. Nakano, D. L. An, K. Tanikawa, K. Wakamatsu, J. Otera, *J. Am. Chem. Soc.* 2004, **126**, 10389.
- [2] S. Hohloch, S. Kaiser, F. L. Duecker, A. Bolje, R. Maity, J. Košmrlj, B. Sarkar, *Dalton trans.* 2015, **44**, 686.
- [3] P. Dierks, A. Pöpcke, O. S. Bokareva, B. Altenburger, T. Reuter, K. Heinze, O. Kühn, S. Lochbrunner, M. Bauer, *Inorg. Chem.* 2020, **59**, 14746.
- [4] a) G. M. Sheldrick, *Acta Cryst.* 2015, **A71**, 3; b) G. M. Sheldrick, *Acta Cryst.* 2015, **C71**, 3.
- [5] H. Oshio, H. Spiering, V. Ksenofontov, F. Renz, P. Gütllich, *Inorg. Chem.* 2001, **40**, 1143.
- [6] M. C. Carey, S. L. Adelman, J. K. McCusker, *Chem. Sci.* 2019, **10**, 134.
- [7] Y. Liu, T. Harlang, S. E. Canton, P. Chábera, K. Suárez-Alcántara, A. Fleckhaus, D. A. Vithanage, E. Göransson, A. Corani, R. Lomoth et al., *Chemical Commun.* 2013, **49**, 6412.
- [8] Y. Liu, K. S. Kjaer, L. A. Fredin, P. Chábera, T. Harlang, S. E. Canton, S. Lidin, J. Zhang, R. Lomoth, K.-E. Bergquist et al., *Chem. Eur. J.* **2015**, **21**, 3628.
- [9] a) E. Livshits, R. Baer, *J. Phys. Chem. A* 2008, **112**, 12789; b) T. Stein, L. Kronik, R. Baer, *J. Am. Chem. Soc.* 2009, **131**, 2818; c) T. Stein, L. Kronik, R. Baer, *J. Chem. Phys.* 2009, **131**, 244119.
- [10] T. Möhle, O. S. Bokareva, G. Grell, O. Kühn, S. I. Bokarev, *J. Chem. Theory and Comput.* 2018, **14**, 5870.
- [11] M. J. Frisch, G. W. Trucks, H. B. Schlegel, G. E. Scuseria, M. A. Robb, J. R. Cheeseman, G. Scalmani, V. Barone, G. A. Petersson, H. Nakatsuji et al., *Gaussian 16 Rev. C.01*, Wallingford, CT, 2016.
- [12] F. Plasser, *J. Chem. Phys.* 2020, **152**, 84108.
- [13] A. Pöpcke, A. Friedrich, S. Lochbrunner, *J. Phys.: Condens. Matter* 2019, **32**, 153001.
- [14] a) R. S. Nicholson, I. Shain, *Anal. Chem.* 1964, **36**, 706; b) J. Heinze, *Angew. Chem.* 1984, **96**, 823.
- [15] J. E. B. Randles, *Trans. Faraday Soc.* 1948, **44**, 327.
- [16] J. N. Demas, E. W. Harris, R. P. McBride, *J. Am. Chem. Soc.* 1977, **99**, 3547.